Journal of Structural Geology 32 (2010) 321–329

Contents lists available at ScienceDirect

Journal of Structural Geology

journal homepage: www.elsevier.com/locate/jsg

Strain analysis of heterogeneous ductile shear zones based on the attitudes of planar markers

Stefano Vitale*, Stefano Mazzoli

Dipartimento di Scienze della Terra, Università degli studi di Napoli 'Federico II', Largo San Marcellino 10, 80138 Napoli, Italy

ARTICLE INFO

Article history:
Received 28 September 2009
Received in revised form
11 December 2009
Accepted 2 January 2010
Available online 14 January 2010

Keywords:
Shear strain
Strain softening
Strain matrix
Wrench zones
Deformed granitoid plutons

ABSTRACT

Using the simple measurement of the attitude of planar features such as foliation, shear planes and displaced tabular markers (such as veins or dykes), fundamental information is obtained on deformation types and rheology in heterogeneous ductile shear zones. The method outlined in this study is based on the subdivision of the shear zone in n deformed layers, each of them being characterized by approximately homogenous deformation. For each layer, paired measurements of θ' and Γ are made, where θ' is the angle that the foliation forms with the shear plane and Γ is the effective shear strain. By means of suitable θ'-Γ grids, constructed according to strain boundary conditions, values of stretch (k), shear strain (γ), strain ratio (R) and kinematic vorticity number (W_k) are calculated. The method has been tested on three ductile wrench zones exposed in a deformed granitoid pluton in the Eastern Alps (Italy). The θ'-Γ data indicate that the shear zones are of dominantly transtensional or transpressional type. Furthermore, the finite shear strain and strain ratio peaked profiles suggest that in all instances shear zone evolution was characterized by strain softening. Analysis of the kinematic vorticity indicates that strain softening essentially affected the simple shear component of the deformation.

1. Introduction

Shear zones are very common structures in the lithosphere and their study is fundamental for investigating heterogeneous rock deformation and strain localization processes (e.g. Ramsay and Graham, 1970; Ramsay, 1980; Ramsay and Huber, 1983, 1987). They are the result of complex interactions between controlling factors such as P-T conditions and fluid behaviour, and a series of parameters including: (i) partitioning of different deformation types (simple shear, pure shear, volume change), (ii) deformation distribution (i.e. degree of strain localization), and (iii) rheology (involving strain softening or strain hardening). The heterogeneous nature of the deformation in most natural shear zones is evident from the variability of finite strain parameters such as strain ratio or shear strain. The origin of strain heterogeneity depends on the evolution of the active shear zone as a function of time (e.g. Means, 1995; Vitale and Mazzoli, 2008).

Most of the strain analysis methods applied to the study of shear zones involve the determination of finite strain ratios, together with the measurement of foliation and shear plane attitudes (θ'-R plot; Fossen and Tikoff, 1993; Vitale and Mazzoli, 2008, 2009). However, the results provided by these techniques often bear large uncertainties because of the difficulties in estimating precisely the finite strain by means of suitable strain markers (such as spherical or ellipsoidal deformed objects). The largest uncertainties are due to the variability of parameters such as object concentration (i.e. the concentration of more competent strain markers embedded in a less competent matrix), viscosity contrast, and object shape (e.g. Treagus and Treagus, 2001; Vitale and Mazzoli, 2005). Furthermore, the most popular methods of finite strain analysis (Fry and Rf/φ techniques; Ramsay, 1967; Fry, 1979; Lisle, 1985) require the fulfilment of a number of assumptions, not always satisfied by rocks. The aim of this paper is to provide an alternative and more precise method for the quantitative analysis of natural shear zones. The proposed method is based on the use of the effective shear strain – rather than finite strain ratio – to characterize heterogeneous deformation in shear zones.

2. θ'-Γ method

The method is based on the analysis of the attitudes of foliation, shear plane and displaced planar markers (e.g. vein, dyke) across the shear zone. Therefore, this technique requires the presence of a well-developed foliation and of a planar marker being intersected by the shear zone (Fig. 1).

* Corresponding author. Tel.: +39 (0) 812538124; fax: +39 (0) 812538338.
E-mail address: stefano.vitale@unina.it (S. Vitale).

0191-8141/$ – see front matter © 2010 Elsevier Ltd. All rights reserved.
doi:10.1016/j.jsg.2010.01.002

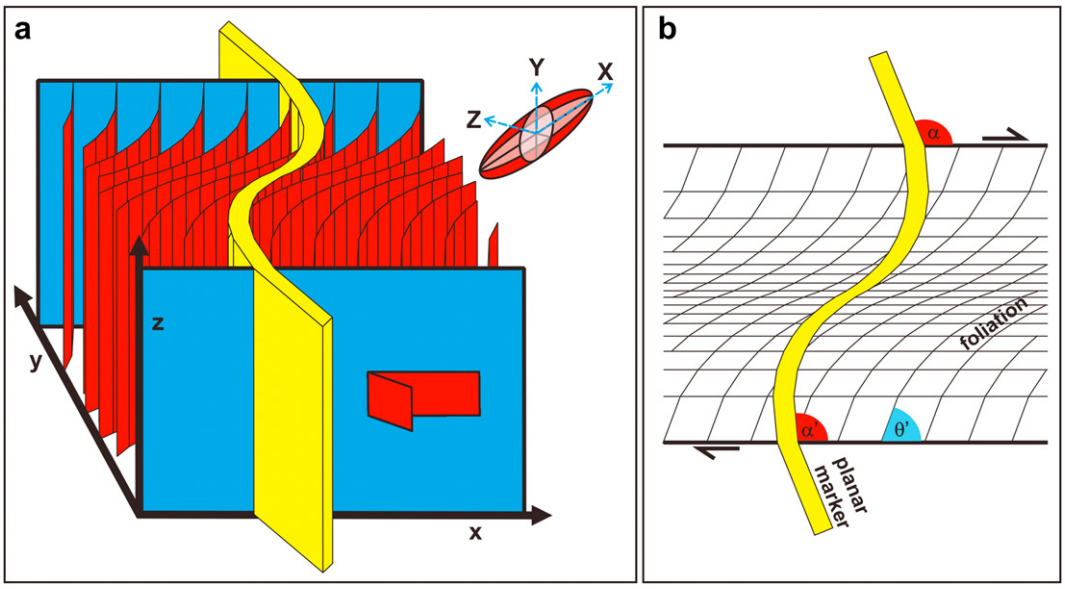

Fig. 1. (a) 3D shear zone model showing the geometric relationship between a deformed planar marker and oblique foliation. The reference frame (*x*, *y*, *z*) used in this study and a schematic orientation of the finite strain ellipsoid (with principal axes: *X*, *Y*, *Z*) are also shown. (b) Shear zone section parallel to the slip vector (xy plane) showing the subdivision into approximately (at the scale of observation) homogeneously deformed layers and the three angles described in the text.

In this study, the shear zone reference frame (Fig. 1a) is indicated by means of lowercase letters (*x*, *y*, *z*, where the *x* axis is parallel to the shear direction and the xz plane is parallel to the shear plane, this being vertical for the analyzed wrench-type shear zones), whereas capital letters (*X*, *Y*, *Z*) are used for the orientation of the principal axes of the finite strain ellipsoid (with the *X* axis parallel to the maximum extension direction and the *Z* axis parallel to the minimum one; e.g. Ramsay and Huber, 1983). The analyzed foliation is assumed to be parallel to the XY plane of the finite strain ellipsoid.

In order to evaluate the effective shear strain Γ (*sensu* Fossen and Tikoff, 1993), the cotangent rule is applied to the displaced planar marker (Eq. 2.3, pg. 24 of Ramsay and Huber, 1983):

$$\Gamma = \cot(\alpha') - \cot(\alpha) \tag{1}$$

where α and α' are the angles between the planar marker and the shear plane in the undeformed host rock and inside the shear zone, respectively (Fig. 1b). In order to collect θ'-Γ data, where θ' is the angle that the foliation forms with the shear plane (Fig. 1b), the heterogeneous ductile shear zone (in this study being of wrench type) is divided into sectors characterized by monotonously increasing or decreasing strain. Each sector, in turn, is divided into *n* suitable layers parallel to the shear plane and characterized by an approximately homogeneous deformation (in others words the finite strain, resulting from a combination of simple shear, pure shear and volume change, is considered as being homogeneous within each layer volume; however, all together the layers define a heterogeneous deformation in which finite strain parameters such as shear strain and stretch values are spatially variable across the shear zone). The thickness of each layer (i.e. the sampling size) notably influences the accuracy of the measurements. Although closer sampling obviously furnishes more precise estimates (the strain within each layer being closer to homogeneous), also choosing layers of constant or variable thickness influences measurement uncertainty. Taking into account that finite strain generally increases in a non-linear fashion from the margins to the centre of a heterogeneous ductile shear zone, logarithmically-spaced sampling is adopted in this study in order to obtain a more homogenous distribution of measurement precision across the shear zone.

Let us assume, for each layer, a deformation characterized by simultaneous simple shear, pure shear and volume change. For the *i*-th layer, the finite strain matrix is in the form (Tikoff and Fossen, 1993):

$$A(i) = \begin{bmatrix} k_1(i) & \Gamma(i) & 0 \\ 0 & k_2(i) & 0 \\ 0 & 0 & k_3(i) \end{bmatrix} \tag{2}$$

where $\Gamma(i) = \gamma(i)(k_1(i) - k_2(i))/\ln(k_1(i)/k_2(i))$ is the *i*-th finite effective shear strain (i.e. the off-diagonal term of the strain matrix), $k_1(i) = (1 + e_1(i))$, $k_2(i) = (1 + e_2(i))$ and $k_3(i) = (1 + e_3(i))$ are the i-th finite stretches, and $e_1(i)$, e_2(i) and $e_3(i)$ are the i-th finite extensions.

Strike-slip deformations may deviate from simple shear because of a component of shortening or extension orthogonal to the deformation zone, determining conditions of transpression or transtension, respectively (*sensu* Dewey et al., 1998). Two cases of transpressional/transtensional wrench zones have been considered in this study:

(a) simple shear in the *xy* plane and synchronous pure shear in the *yz* plane (i.e. $k_1 = 1$ and $k_3 = k_2^{-1}$), represented by the strain matrix (Fossen and Tikoff, 1993):

$$A_1 = \begin{bmatrix} 1 & \gamma\frac{(1-k_2)}{\ln(1/k_2)} & 0 \\ 0 & k_2 & 0 \\ 0 & 0 & 1/k_2 \end{bmatrix} \tag{3}$$

(b) simple shear and synchronous pure shear, both in the *xy* plane (i.e. $k_3 = 1$ and $k_1 = k_2^{-1}$), represented by the strain matrix:

$$A_2 = \begin{bmatrix} 1/k_2 & \gamma\frac{(1/k_2-k_2)}{\ln(1/k_2^2)} & 0 \\ 0 & k_2 & 0 \\ 0 & 0 & 1 \end{bmatrix} \tag{4}$$

In cases where pure shear is localized within the shear zone only (i.e. it does not involve the host rock), vertical or horizontal stretching occurs for cases (a) and (b) above, respectively (Sanderson and Marchini, 1984; Jones et al., 1997; Dewey et al., 1998).

Grids for plotting the θ'-Γ data (Fig. 2) may be constructed by allowing the values of k_2 and γ vary in the following equations (Fossen and Tikoff, 1993; Tikoff and Fossen, 1993):

$$\Gamma = \frac{\gamma(k_1 - k_2)}{\ln\left(\frac{k_1}{k_2}\right)} \tag{5}$$

$$\theta' = arctan\left(-\frac{\Gamma_2 + k_2 - \lambda_{max}}{k_2\Gamma}\right) \tag{6}$$

where λ_{max} is the maximum one among the three eigenvalues of the matrix $A_1A_1^T$ (i.e. the lengths of the finite strain ellipsoid axes):

$$\lambda_{1,2,3} = \begin{Bmatrix} \frac{1}{2}\left(\Gamma^2 + 1 + k_2^2 + \sqrt{-4k_2^2 + \left(\Gamma^2 + 1 + k_2^2\right)^2}\right) \\ \frac{1}{2}\left(\Gamma^2 + 1 + k_2^2 - \sqrt{-4k_2^2 + \left(\Gamma^2 + 1 + k_2^2\right)^2}\right) \\ k_2^{-2} \end{Bmatrix} \tag{7}$$

and the matrix $A_2A_2^T$:

$$\lambda_{1,2,3} = \begin{Bmatrix} \frac{1}{2}\left(\Gamma^2 + k_2^{-2} + k_2^2 + \sqrt{-4 + \left(\Gamma^2 + k_2^{-2} + k_2^2\right)^2}\right) \\ \frac{1}{2}\left(\Gamma^2 + k_2^{-2} + k_2^2 - \sqrt{-4 + \left(\Gamma^2 + k_2^{-2} + k_2^2\right)^2}\right) \\ 1 \end{Bmatrix} \tag{8}$$

In order to obtain the mathematical value of the stretch k_2 from the Γ-θ' data for transpressional/transtensional wrench zones in the case (a) above, the λ_{max} value (in this case being λ_1) in Eq. (7) is replaced with that obtained from Eq. (6). Then, using the equation:

$$2\left(\Gamma^2 + 1 + k_2\tan\theta'\right) - \left(\Gamma^2 + 1 + k_2^2 + \sqrt{-4k_2^2 + \left(\Gamma^2 + 1 + k_2^2\right)^2}\right) = 0$$

having a solution:

$$k_2 = \frac{-\Gamma + \Gamma\tan\theta' + \sqrt{\Gamma^2 + 2\Gamma^2\tan^2 4\theta' + \Gamma^2\tan^4\theta' + 4\Gamma^2\tan^2\theta'}}{2\tan\theta'} \tag{10}$$

shear strain values can be obtained by means of Eq. (5).

In a general case, where it is difficult to find a resolvable equation, it is possible to graphically obtain values of stretch (k) and shear strain (γ) by means of a suitable θ'-Γ grid, constructed according to strain boundary conditions.

3. Application of the θ'-Γ method: shear zones in the Neves Lake area (Eastern Alps)

The study area (Fig. 3a) is that intensely investigated by Mancktelow and Pennacchioni (2005) and Pennacchioni and Mancktelow (2007), whose papers provide comprehensive and detailed accounts of both regional geological setting and spectacular shear zones exposed on a surface previously polished by a glacier. As demonstrated by the latter Authors, the analyzed shear zones are exposed in a low-strain domain of an elsewhere extensively deformed and mylonitized, pre-Alpine intrusive granitoid body included within the amphibolite facies 'Zentralgneiss' (Penninic units exposed within the Tauern tectonic window, Eastern Alps). Shear zone nucleation was controlled by the presence of precursor joints, and occurred by a widespread reactivation process characterizing solid-state deformation of granitoid plutons also elsewhere (e.g. Pennacchioni, 2005; Mazzoli et al., 2009).

For this study, three shear zones have been selected. From the least to the most evolved, they have been named: SZ1, SZ2, and SZ3. The shear zones are characterized by a well-developed foliation and by the presence of deformed quartz veins that are intersected by the shear zones themselves (Fig. 3b–d). As demonstrated by Mancktelow and Pennacchioni (2005) and Pennacchioni and Mancktelow (2007) based on the detailed analysis of a large number of structures, wrench zones are about vertical and are characterized by sub-horizontal slip vectors and dextral sense of shear, with deformation involving no volume variation. For the analyzed structures, shear zone thickness ranges from 14 (SZ1) to 2.5 cm (SZ3) and quartz vein thickness varies from 9 to 10 (SZ1, SZ2) to about 1 cm (SZ3). SZ3 actually consists of two parallel, closely spaced but distinct, 'paired' (Mancktelow and Pennacchioni, 2005) shear zones (Fig. 3d). Roughly N-S striking quartz veins in the study area may locally accommodate minor, vein-parallel sinistral shear (Pennacchioni and Mancktelow, 2007). However, for the structures

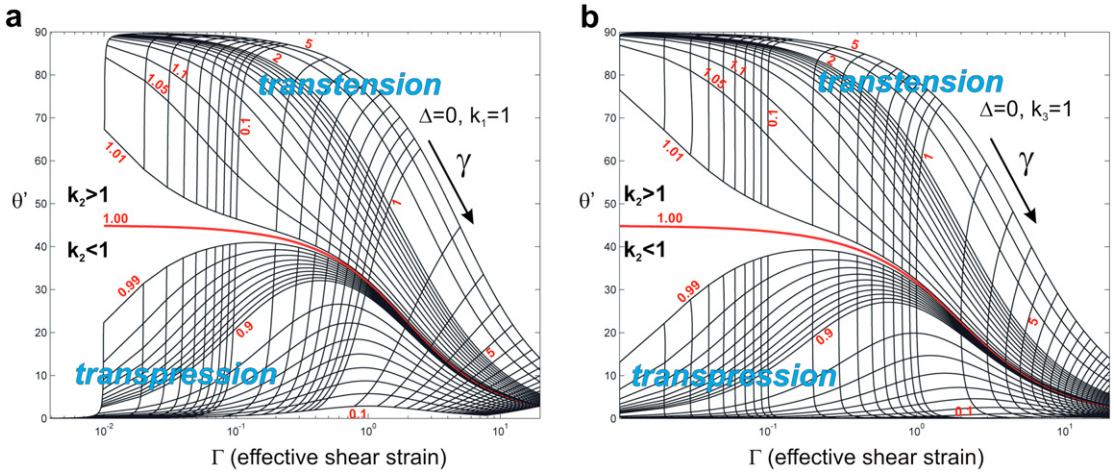

Fig. 2. Examples of θ'-Γ grids for transpressional/transtensional wrench zones. (a) $\Delta = 0$, $k_1 = 1$. (b) $\Delta = 0$, $k_3 = 1$.

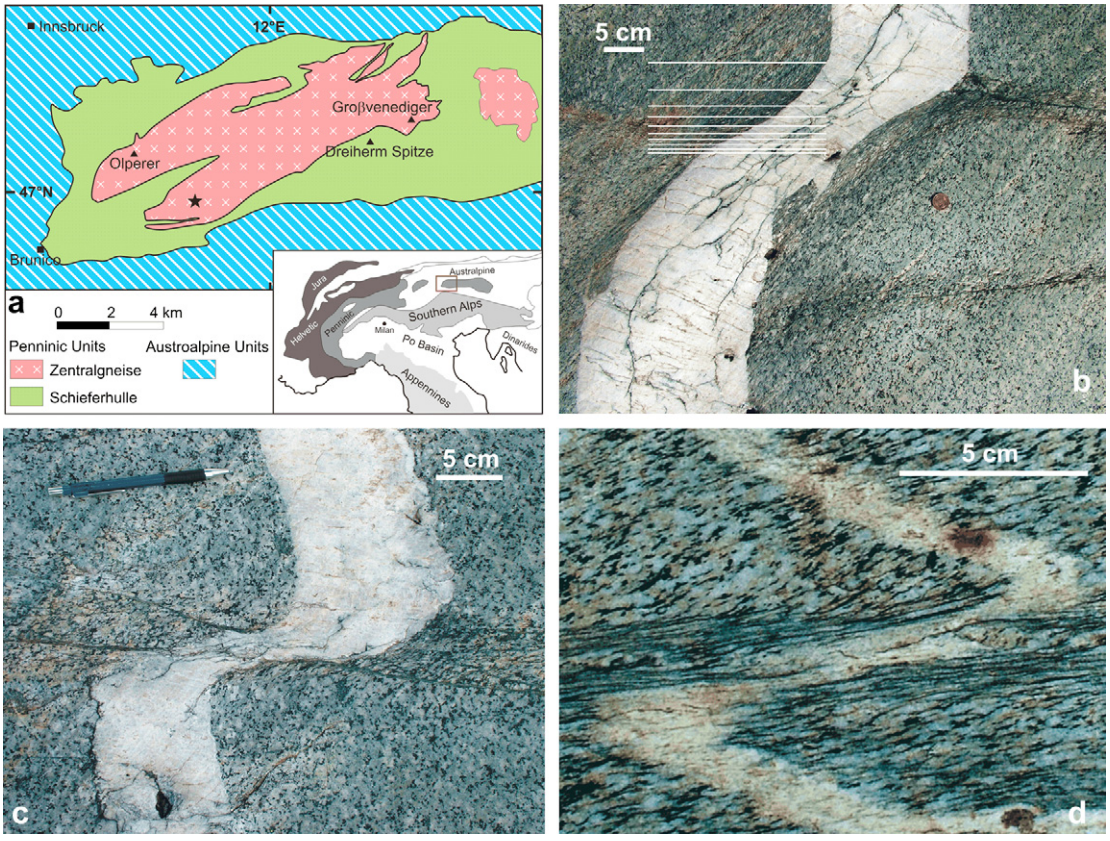

Fig. 3. Location of field study area and outcrop view of studied dextral ductile wrench zones deforming quartz veins. (a) Simplified geological map of part of the Eastern Alps, showing site of structural analysis (star) NE of the Neves Lake (after Pennacchioni and Mancktelow, 2007). (b) Low-shear strain zone (SZ1), showing example of logarithmic-sized sampling grid. (c) Moderate-shear strain zone (SZ2). (d) High-shear strain zone (SZ3).

analyzed in this study (Fig. 3b–d) vein-parallel simple shear appears to be negligible. Therefore, quartz veins are treated as passive markers.

In order to collect θ'-Γ data, the analyzed shear zones have been divided into approximately homogeneously deformed, logarithmically-spaced parallel layers (see example in Fig. 3b). For each shear zone, sets of measurements have been collected from two transects located on the right-hand and left-hand sides of the quartz vein deformed within the shear zone. The following parameters have been recorded (by image analysis): (i) thickness (T) of each layer; (ii) angle θ' that the foliation forms with the shear plane; (iii) angle α' that the quartz vein forms with the shear plane; (iv) angle α between the shear plane and the vein outside the shear zone. By means of these quantities, the i-th finite effective shear strain $\Gamma(i)$ may be obtained.

By using Eq. (1), the finite effective shear strain (Γ) has been calculated and plotted versus shear zone thickness (T) for the three analyzed structures (Fig. 4a, b, e, f, i, j). Γ-profiles display asymmetric peaked shapes with a single maximum (occurring on both sides of the quartz vein) for SZ1, one maximum (right side) and two maxima (left side) for SZ2, and two maxima for SZ3 (both sides).

In order to obtain information on finite stretches and shear strains, θ'-Γ data have been plotted on a grid constructed for $\Delta = 0$ and for the two cases of $k_1 = 1$ or $k_3 = 1$ (Fig. 4c, d, g, h, k, l). It is worth noting that, for both cases, most of SZ1-data fall in the transtension field, with a strain path characterized by a decrease of stretch as the shear strain increases, eventually entering the transpression field (Fig. 4c–d). Also SZ2-data plot in both transtension and transpression fields, with a trend similar to the previous one, for both cases of $k_1 = 1$ or $k_3 = 1$ (Fig. 4g–h). On the contrary, most of SZ3-data fall in the transpression field (Fig. 4k–l). These data are also indicative of higher values of finite shear strain.

For each layer within the analyzed shear zones, values of stretch (k_2) and shear strain (γ) have been obtained either by means of Eqs. (7) and (3) (in the case of $\Delta = 0$ and $k_1 = 1$) or graphically (in the case of $\Delta = 0$ and $k_3 = 1$).

In order to gain information on the partitioning between simple and pure shear components of the finite strain, the kinematic vorticity number (W_k) has been estimated by means of equation (Tikoff and Fossen, 1993):

$$W_k = \cos\left\{\arctan\left[\frac{2\ln(k_2)}{\gamma}\right]\right\} \tag{11}$$

Profiles of finite shear strain (γ), strain ratio (R_{XZ}), stretch (k_2) and kinematic vorticity number (W_k) across the three studied shear zones are displayed in Figs. 5(a–l) and 6(a–l) for the cases of $\Delta = 0$, $k_1 = 1$, and $\Delta = 0$, $k_3 = 1$, respectively. Kinematic vorticity number (W_k) is plotted versus finite shear strain (γ) in the diagrams of Figs. 5(m–o) and 6(m–o).

4. Discussion

The three analyzed shear zones are characterized by heterogeneous finite strain, clearly marked by the peaked profiles of finite effective shear strain (Fig. 4a, b, e, f, i, j), shear strain (Figs. 5a–c and 6a–c) and strain ratio (Figs. 5d–f and 6d–f). The analyzed structures are characterized by different states of deformation, ranging from weak (SZ1; $\Gamma_{max} = 2$), to moderate (SZ2; $\Gamma_{max} = 17$), to high (SZ3; $\Gamma_{max} = 50$). The peaked strain profiles suggest that a strain

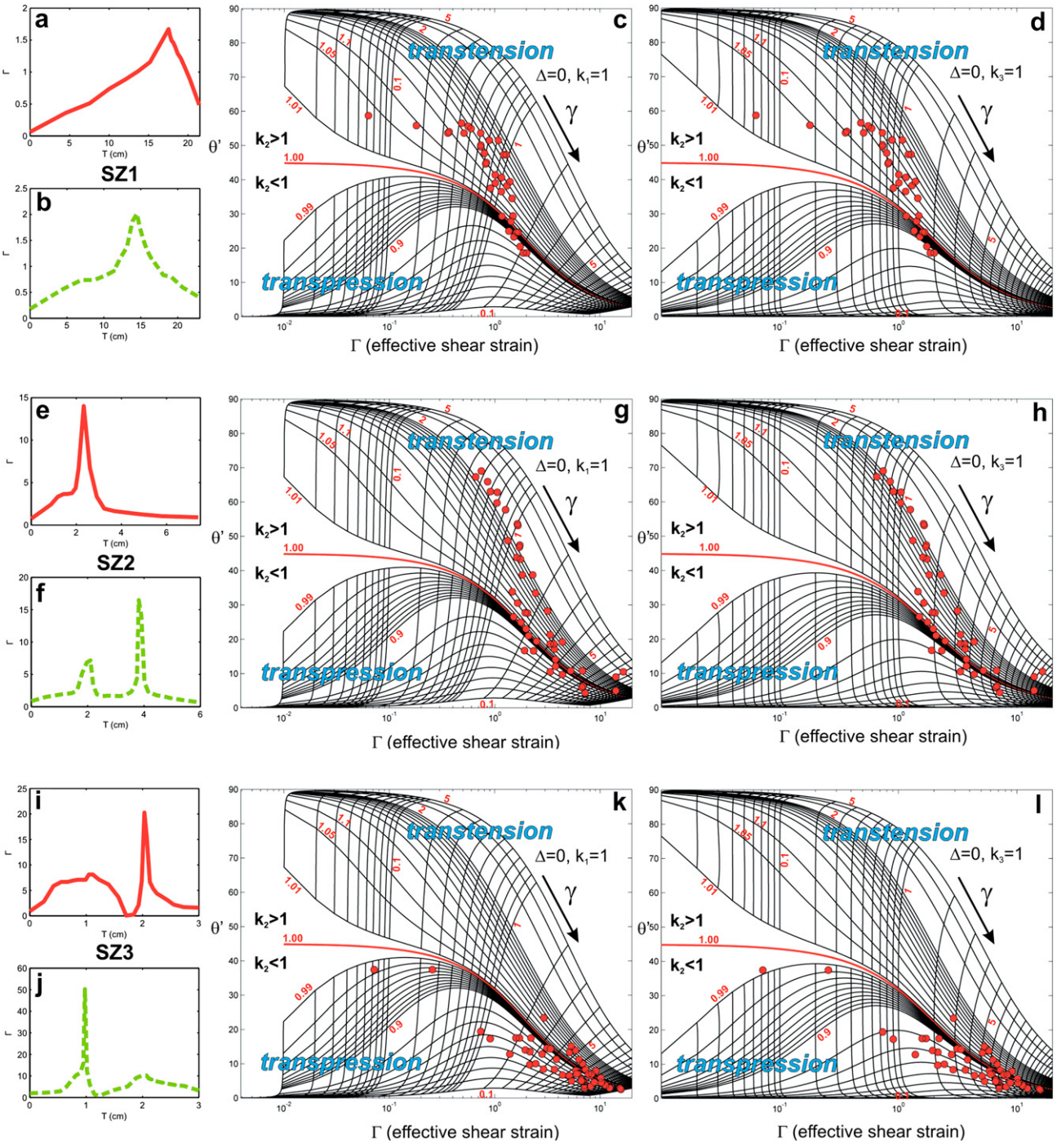

Fig. 4. Diagrams of finite effective shear strain (Γ) vs. shear zone thickness (T) (profiles located on both right-hand and left-hand sides of the quartz vein deformed within each shear zone), and θ'-Γ plots (constructed for the condition of $\Delta = 0$; see text). (a) Right-hand side of SZ1. (b) Left-hand side of SZ1. (c) θ'-Γ plot for SZ1 in the case of $k_1 = 1$. (d) θ'-Γ plot for SZ1 in the case of $k_3 = 1$. (e) Right-hand side of SZ2. (f) Left-hand side of SZ2. (g) θ'-Γ plot for SZ2 in the case $k_1 = 1$. (h) θ'-Γ plot for SZ2 in the case of $k_3 = 1$. (i) Right-hand side of SZ3. (j) Left-hand side of SZ3. (k) θ'-Γ plot for SZ3 in the case of $k_1 = 1$. (l) θ'-Γ plot for SZ3 in the case of $k_3 = 1$.

softening rheology controls the temporal development of the studied shear zones (Means, 1984, 1995; Vitale and Mazzoli, 2008). In fact, strain softening allows the inner part of the shear zone to accumulate more strain with respect to the margins that become inactive with time. Strain softening implies variable shear strain rates and/or longitudinal strain rates, meaning that deformation was not of steady-state type.

Taking into account the available constraint on deformation involving no volume change (Mancktelow and Pennacchioni, 2005; Pennacchioni and Mancktelow, 2007), our analysis reveals that deformation generally deviates from simple shear due to a component of extension or shortening orthogonal to the analyzed ductile wrench zones, determining conditions of transtension or transpression. Two of the analyzed shear zones (SZ1 and SZ2) are characterized by prevalent transtension (which however decreases as the finite shear strain increases, eventually switching to transpression; Fig. 4c, d, g, h), whereas SZ3 records dominant transpressional deformation and higher values of finite shear strain (Fig. 4k, l). All three cases are characterized by a variable component of the intermediate finite stretch (k_2) (Figs. 5g–i and 6g–i).

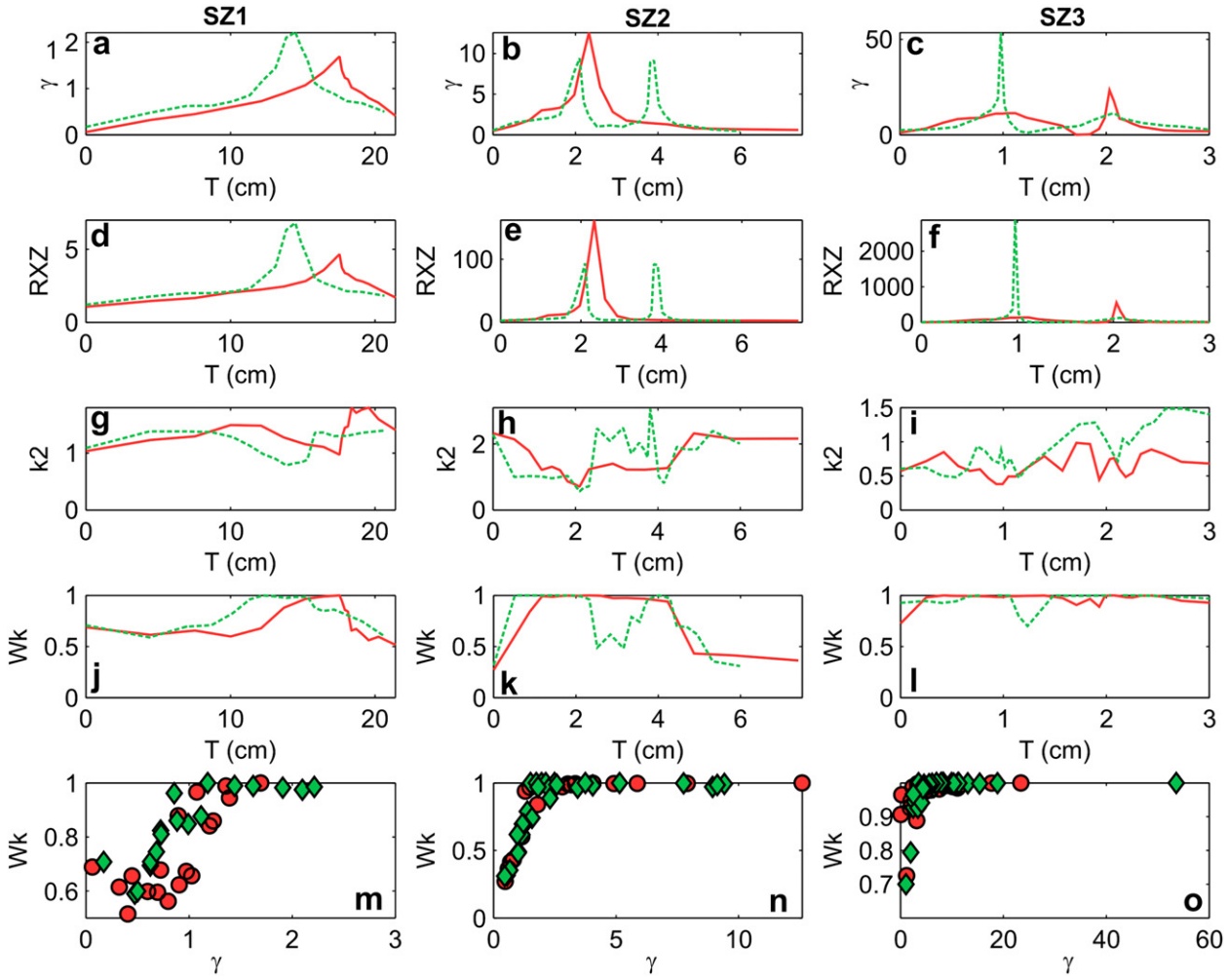

Fig. 5. Transpressional/transtensional wrench zones with pure shear in the yz plane (i.e. $\Delta = 0$, $k_1 = 1$). (a–c) Plots of finite shear strain (γ) vs. shear zone thickness (T). (d–f) Plots of finite strain ratio (R_{XZ}) vs. shear zone thickness (T). (g–i) Plots of finite stretch (k_2) vs. shear zone thickness (T). (j–l) Plots of kinematic vorticity number (W_k) vs. shear zone thickness (T). (m–o) Plots of kinematic vorticity number (W_k) vs. finite shear strain (γ). Symbols: solid lines and circles refer to the right-hand side of the deformed planar marker, dotted lines and diamonds refer to left-hand side.

However, deformation along the intermediate axis of the finite strain ellipsoid tends to disappear ($k_2 = 1$) for high values of finite shear strain.

The partitioning between simple shear and pure shear components across the shear zones is recorded by the kinematic vorticity number (W_k), which mainly ranges between 0.5 and 1 (Figs. 5j–l and 6j–l). It is worth noting that plotting the kinematic vorticity number against the finite shear strain (Figs. 5m–o and 6m–o) indicates a negligible pure shear component of the deformation ($W_k \approx 1$) for high values of shear strain.

In order to better emphasize the relationship between finite shear strain, stretch (k_2) and kinematic vorticity number, γ-k_2 data for each shear zone have been plotted on a semi-logarithmic diagram including W_k isolines (Fossen and Tikoff, 1993). The diagrams (Fig. 7) are divided into three fields according to principal finite strain ellipsoid axis orientation. For low values of finite shear strain ($\gamma < 1.5$), in both strain configurations ($\Delta = 0$, $k_1 = 1$, Fig. 7a; and $\Delta = 0$, $k_3 = 1$, Fig. 7b) most of the data fall into the transtension field, with the finite stretch (k_2) value ranging between 1 and 5, and kinematic vorticity number ranging between 0.4 and 1. In this case, finite strain ellipsoids may be characterized by a vertical Z axis and horizontal X and Y axes (i.e. horizontal foliation). Only a few data plotting into the transpression field are characterized by a vertical X axis and horizontal Y and Z axes. For high values of finite shear strain ($1.5 < \gamma < 50$), most of the data display a kinematic vorticity number close to unity ($W_k > 0.9$), finite stretch (k_2) values ranging between 0.6 and 2, and finite strain ellipsoids both in the transtensional and transpressional field, with a vertical Y axis and horizontal X and Z axes (i.e. vertical foliation). All these features corroborate the hypothesis that the heterogeneous strain observed in these transtensional/transpressional shear zones is probably the result of a strain softening process that affected the simple shear component only, whereas the pure shear component of the deformation becomes more and more negligible from the margins to the centre of the wrench zone.

Finite strain ratios have been plotted in Ramsay's (1967) logarithmic diagram (modification of the well known Flinn diagram; Flinn, 1962) for finite strain ellipsoids classification, only in the case of $k_1 = 1$ and $k_3 = k_2^{-1}$, as deformation characterized by $k_3 = 1$ and $k_1 = k_2^{-1}$ is of plane strain type (non-coaxial plane strain *sensu* Jones et al., 1997) and all the related ellipsoids would plot along the diagram bisector. Finite strain ellipsoids determined for weakly to moderately deformed rocks from prevalently transtensional shear zones (SZ1 and SZ2) fall into the prolate field, whereas most of the dominantly transpressional, high-strain shear zone (SZ3) finite strain ellipsoids plot into the oblate sector (Fig. 8).

The transpressional character of SZ3 is probably related to homogeneous deformation affecting both the host rock and the

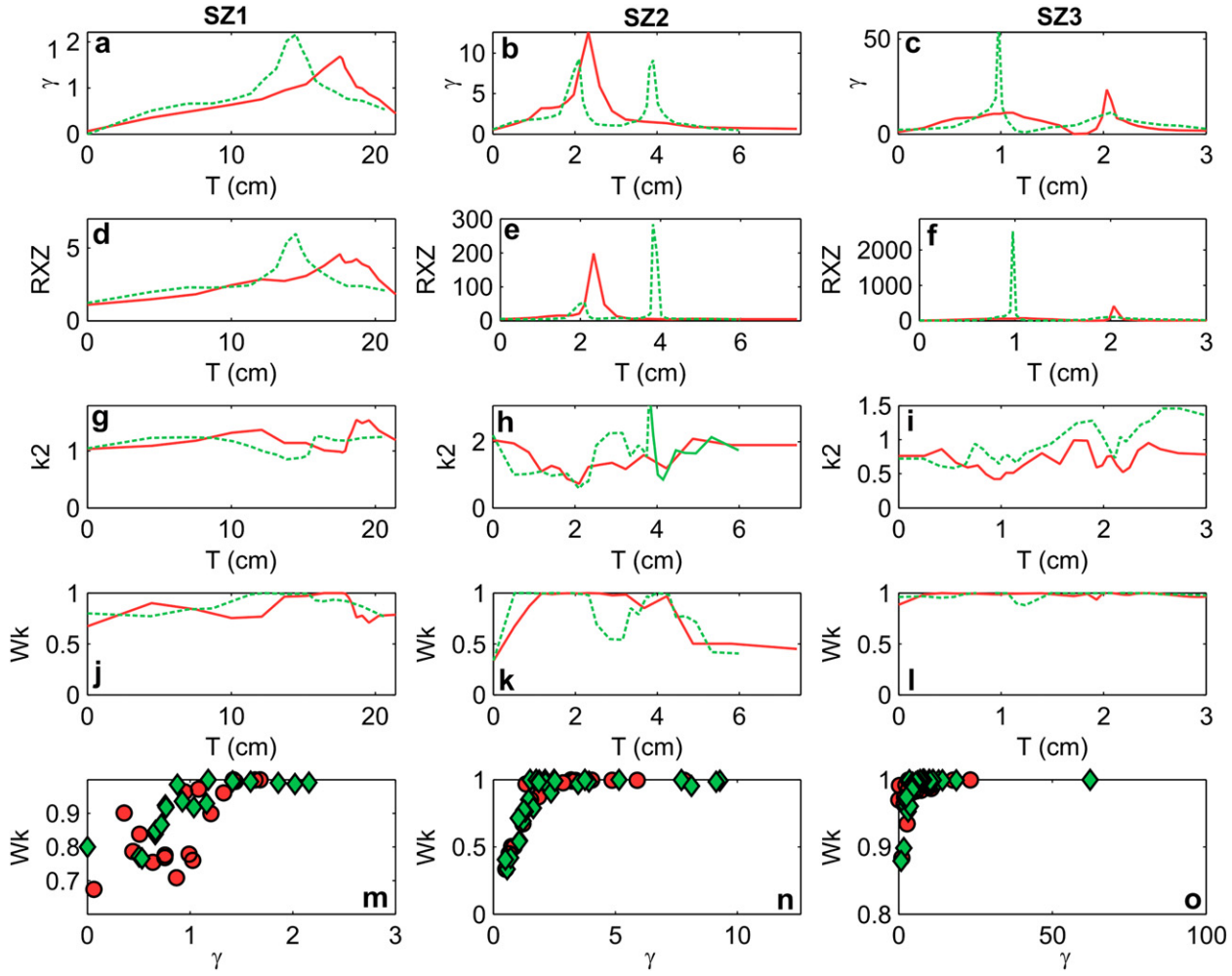

Fig. 6. Transpressional/transtensional wrench zones with pure shear in the xz plane (i.e. $\Delta = 0$, $k_3 = 1$). (a–c) Plots of finite shear strain (γ) vs. shear zone thickness (T). (d–f) Plots of finite strain ratio (R_{XZ}) vs. shear zone thickness (T). (g–i) Plots of finite stretch (k_2) vs. shear zone thickness (T). (j–l) Plots of kinematic vorticity number (W_k) vs. shear zone thickness (T). (m–o) Plots of kinematic vorticity number (W_k) vs. finite shear strain (γ). Symbols: solid lines and circles refer to the right-hand side of the deformed planar marker, dotted lines and diamonds refer to left-hand side.

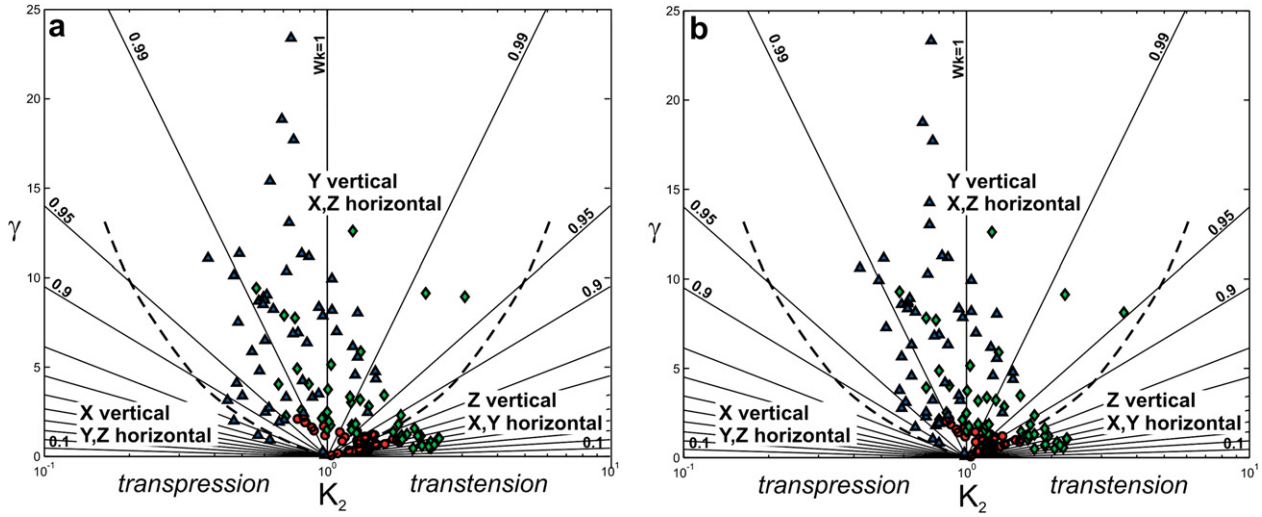

Fig. 7. (a–b) Data from the analyzed shear zones plotted on the γ-k_2 diagram of Fossen and Tikoff (1993) for transpressional/transtensional wrench zone characterized by $\Delta = 0$, $k_1 = 1$ (a), and $\Delta = 0$, $k_3 = 1$ (b). Symbols: circles, diamonds and triangles refer to SZ1, SZ2, and SZ3, respectively.

shear zone, with roughly horizontal maximum shortening oriented at a low angle to the vein plane in the host rock (Fig. 3d). As suggested by Pennacchioni and Mancktelow (2007), this homogeneous strain may be coeval with localized simple shear. In contrast, for SZ1 and SZ2 no appreciable homogeneous strain can be observed in the host rock (Fig. 3b, c); deformation within these shear zones shows a transtensional character for low shear strain values, moving toward the transpression field as shear strain increases (Fig. 4c, d, g, h). Therefore, it appears that SZ1 and SZ2 are characterized by localized, coupled simple shear and pure shear within an essentially undeformed host rock, whereas SZ3 records a dominant localization of the simple shear component within the context of a bulk homogeneous deformation (Fig. 4k–l).

The method proposed in this study has been applied to wrench zones characterized by no volume change. However, this technique can be used for any strain configuration, such as those characterizing thrust zones, as well as wrench zones (Fossen and Tikoff, 1993), and for any type of strain including a simultaneous combination of simple shear with a three-dimensional coaxial deformation involving apparent constriction ($\Delta > 0$), apparent flattening ($\Delta < 0$), or pure shear with no volume change (Tikoff and Fossen, 1999). According to the specific boundary conditions, it is possible to construct appropriate grids allowing one to obtain, graphically or mathematically, the shear strain and stretches values. It should be noted that, for most of the data, the *Y* axis of the finite strain ellipsoid is vertical (Fig. 7), hence the *XY* plane – and the foliation that is assumed to be parallel to it – are also vertical. Only for the shear zone margins, where the shear strain is very low, the *XY* plane may be horizontal, making hard to recognize the foliation and increasing measurement uncertainties. On the other hand, where the foliation is well developed – that is in the centre of the shear zone – little variations of the angle θ' imply large variations of the obtained values of stretch and shear strain (see the θ'-Γ diagrams of Fig. 4). Therefore, particular care has to be taken in the measurement of the angle θ', especially for those shear zone sectors recording lowest deformation, on one extreme, and highest deformation on the other.

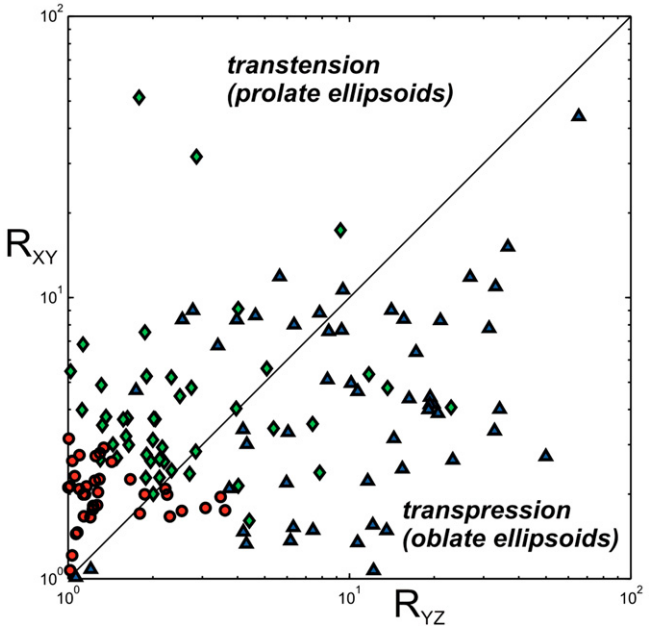

Fig. 8. Data from the analyzed shear zones plotted on the Ramsay diagram for finite strain ellipsoid classification; transpressional/transtensional wrench zones are characterized by $\Delta = 0$, $k_1 = 1$. Symbols: circles, diamonds and triangles refer to SZ1, SZ2, and SZ3, respectively.

5. Conclusions

The method presented in this study delivers, in a relatively easy and handy way, fundamental information on finite strain characteristics in shear zones. The simple measurement of three angles (θ', α', and α) permits the calculation of the finite effective shear strain (Γ), the construction of the θ'-Γ plot (displaying the relationship between finite effective shear strain and the angle that the foliation forms with the shear plane), and to obtain information on finite values of stretch and shear strain. The only necessary conditions required to apply this method are the occurrence of a well-developed foliation and a deformed planar marker, and the care to measure all structures parallel to the simple shear plane of the coordinate frame defined in this study with reference to the shear zone.

The proposed method has been applied to the study of three ductile wrench zones exposed in deformed granitoid rocks of the Eastern Alps, for which additional information about volume change during deformation ($\Delta = 0$) were available (Mancktelow and Pennacchioni, 2005; Pennacchioni and Mancktelow, 2007). Assuming that these strike-slip shear zones may be characterized by transpressional or transtensional deformation, the finite values of stretch and shear strain have been determined across the shear zones. The obtained gradients of finite strain parameters such as stretch (k_2), shear strain (γ), strain ratio (R_{XZ}), effective shear strain (Γ), and kinematic vorticity number (W_k) provide all the information needed to fully characterize the deformation. In our case, it is possible to establish that the analyzed heterogeneous ductile shear zones are characterized by dominant transtensional or transpressional type of deformation. Analysis of the finite simple shear component, which increases from the margins toward the centre of the shear zones, suggests that strain softening processes significantly affected the non-coaxial component of the deformation. On the other hand, the finite pure shear component of the deformation attains a variable intensity and tends to disappear for high values of finite strain, high-strain shear zones being essentially characterized by non-coaxial strain. Our results also suggest heterogeneous partitioning of the deformation in the rock: localization of both simple shear and pure shear strain is recorded by two analyzed shear zones (SZ1 and SZ2), whereas dominant localization of the simple shear component occurred in the third, higher-strain shear zone (SZ3) that evolved within the framework of a bulk coaxial strain affecting the whole rock volume.

Acknowledgments

We sincerely thank Giorgio Pennacchioni for having led us in 'his' field area NE of the Neves Lake, Eastern Alps, where he has carried out an incredible amount of detailed work over several years.

Constructive comments by Richard Lisle and JSG Editor Joao Hippertt helped us to substantially improve the paper.

References

Dewey, J.F., Holdsworth, R.E., Strachan, R.A., 1998. Transpression and transtension zones. In: Geological Society, London, Special Publications, vol. 135, pp. 1–14. doi:10.1144/GSL.SP.1998.135.01.01.

Flinn, D., 1962. On folding during three-dimensional progressive deformation. In: Quarterly Journal of Geological Society of London, vol. 118, pp. 385–428.

Fossen, H., Tikoff, B., 1993. The deformation matrix for simultaneous simple shearing, pure shearing and volume change, and its application to transpression-transtension tectonics. Journal of Structural Geology 15, 413–422.

Fry, N., 1979. Random point distributions and strain measurement in rocks. Tectonophysics 60, 89–105.

Jones, R.R., Holdswoth, R.E., Bailey, W., 1997. Lateral extrusion in transpression zones: the importance of boundary conditions. Journal of Structural Geology 19, 1201–1217.

Lisle, R.J., 1985. Geological Strain Analysis: A Manual for the Rf/φ Technique. Pergamon, Oxford, pp. 95.
Mancktelow, N.S., Pennacchioni, G., 2005. The control of precursor brittle fracture and fluid – rock interaction on the development of single and paired ductile shear zones. Journal of Structural Geology 27, 645–661.
Mazzoli, S., Vitale, S., Delmonaco, G., Guerriero, V., Margottini, C., Spizzichino, D., 2009. 'Diffuse faulting' in the Machu Picchu granitoid pluton, Eastern Cordillera, Peru. Journal of Structural Geology 31, 1395–1408. doi:10.1016/j.jsg.2009.08.010.
Means, W.D., 1984. Shear zones of types I and II and their significance for reconstruction of rock history. In: Geological Society of America Abstracts, vol. 16, p. 50.
Means, W.D., 1995. Shear zones and rock history. Tectonophysics 247, 157–160.
Pennacchioni, G., 2005. Control of the geometry of precursor brittle structures on the type of ductile shear zone in the Adamello tonalites, Southern Alps (Italy). Journal of Structural Geology 27, 627–644.
Pennacchioni, G., Mancktelow, N.S., 2007. Nucleation and initial growth of a shear zone network within compositionally and structurally heterogeneous granitoids under amphibolite facies conditions. Journal of Structural Geology 29, 1757–1780. doi:10.1016/j.jsg.2007.06.002.
Ramsay, J.G., 1967. Folding and Fracturing of Rocks. McGraw-Hill, New York.
Ramsay, J.G., 1980. Shear zone geometry: a review; shear zones in rocks. Journal of Structural Geology 2, 83–99.
Ramsay, J.G., Graham, R.H., 1970. Strain variation in shear belts. Canadian Journal of Earth Sciences 7, 786–813.
Ramsay, J.G., Huber, M., 1983. The techniques of modern structural Geology. In: Strain Analysis, vol. I. Academic Press, London.
Ramsay, J.G., Huber, M., 1987. The techniques of modern structural Geology. In: Folds and Fractures, vol. II. Academic Press, London.
Sanderson, D., Marchini, R.D., 1984. Transpression. Journal of Structural Geology 6, 449–458.
Tikoff, B., Fossen, H., 1993. Simultaneous pure and simple shear: the unified deformation matrix. Tectonophysics 217, 267–283.
Tikoff, B., Fossen, H., 1999. Three-dimensional deformations and strain facies. Journal of Structural Geology 21, 1497–1512.
Treagus, S.H., Treagus, J.E., 2001. Effects of object ellipticity on strain, and implications for clast – matrix rocks. Journal of Structural Geology 23, 601–608.
Vitale, S., Mazzoli, S., 2005. Influence of object concentration on finite strain and effective viscosity contrast: insights from naturally deformed packstones. Journal of Structural Geology 27, 2135–2149.
Vitale, S., Mazzoli, S., 2008. Heterogeneous shear zone evolution: the role of shear strain hardening/softening. Journal of Structural Geology 30, 1363–1395.
Vitale, S., Mazzoli, S., 2009. Finite strain analysis of a natural ductile shear zone in limestones: insights into 3-D coaxial vs. non-coaxial deformation partitioning. Journal of Structural Geology 31, 104–113.